

Numerical Heat Transfer, Part A: Applications

An International Journal of Computation and Methodology

ISSN: 1040-7782 (Print) 1521-0634 (Online) Journal homepage: <http://www.tandfonline.com/loi/unht20>

MHD phase change heat transfer in an inclined enclosure: Effect of a magnetic field and cavity inclination

Mohammad Ghalambaz, Ali Doostanidezfuli, Hossein Zargartalebi & Ali J. Chamkha


To cite this article: Mohammad Ghalambaz, Ali Doostanidezfuli, Hossein Zargartalebi & Ali J. Chamkha (2017): MHD phase change heat transfer in an inclined enclosure: Effect of a magnetic field and cavity inclination, Numerical Heat Transfer, Part A: Applications

To link to this article: <http://dx.doi.org/10.1080/10407782.2016.1244397>



Published online: 06 Jan 2017.



Submit your article to this journal 



View related articles 



View Crossmark data 

MHD phase change heat transfer in an inclined enclosure: Effect of a magnetic field and cavity inclination

Mohammad Ghalambaz^a, Ali Doostanidezfuli^a, Hossein Zargartalebi^b, and Ali J. Chamkha^{c,d}

^aDepartment of Mechanical Engineering, Dezful Branch, Islamic Azad University, Dezful, Iran; ^bDepartment of Mechanical Engineering, Shahid Chamran University of Ahvaz, Ahvaz, Iran; ^cMechanical Engineering Department, Prince Mohammad Bin Fahd University, Al-Khobar, Kingdom of Saudi Arabia; ^dPrince Sultan Endowment for Energy and Environment, Prince Mohammad Bin Fahd University, Al-Khobar, Kingdom of Saudi Arabia

ABSTRACT

The MHD phase change heat transfer of a phase change substance in the presence of a uniform magnetic field is theoretically studied in a cavity. A fixed grid method associated with the enthalpy–porosity method is utilized. The governing equations are transformed into a non-dimensional form and solved using the finite element method. The impacts of the crucial parameters such as the Hartmann number and the inclination angle on the phase change process are investigated. It is found that any increase in Hartmann number and the inclination angle of the cavity leads to a decrease in the rate of the melting process.

ARTICLE HISTORY

Received 9 June 2016
Accepted 16 September 2016

1. Introduction

Solid–liquid phase change processes play a crucial role in metallurgical industries, particularly in extraction and fabrication operations. Therefore, modeling of such processes has drawn investigators' attention to study this phenomenon by carrying out analytical, numerical, and experimental researches. These processes involve heat and mass transfer phenomena and thus, the capability to comprehend the interaction between the phase change phenomenon and the fluid flow, solidification models, and the heat transfer in multicomponent systems is of interest recently. As a result, multifarious investigations have been implemented involving experimental and theoretical modeling of phase change problems [1–3]. Accordingly, due to the fact that conserving thermal energy is really challenging, utilizing latent heat storage, as one of the most efficient ways in this regard, is of paramount importance to researchers. In actual fact, phase change materials (PCM) have the potential to absorb–release significant latent heat in the course of the solidifying–melting procedure. Consequently, several investigators have studied numerous problems pertinent to PCM modeling. Duan et al. [4], considering an enthalpy formulation of energy equation, implemented a numerical study of the solidification of a pure n-hexadecane into a cavity. The impacts of different parameters such as aspect ratio of the rectangular cavity, initial liquid superheat, and cold wall temperature were studied in terms of the solid fraction and the shape of solid–liquid phase front. Semma et al. [5] adopted the lattice Boltzmann method to study melting and solidification problems. Utilizing two distribution function approaches and D2Q9 lattice, they solved two-dimensional fluid flow and heat transfer. Moreover, they traced the phase interface by applying partial or probabilistic bounce back approach and compared the predicted solutions for phase change problems with the conventional methods. Wang et al. [6] conducted a comprehensive numerical model for melting with natural convection.

CONTACT Mohammad Ghalambaz ✉ m.ghalambaz@iaud.ac.ir Assistant Professor, Mechanical Engineering Department, Dezful Branch, Islamic Azad University, Dezful, Iran.

Color versions of one or more of the figures in the article can be found online at www.tandfonline.com/unht.

Nomenclature

A_{mush}	mushy-zone constant (Carman–Koseny equation constant)	v	velocity in the y -direction (m/s)
a	enclosure inclination angle	α	thermal diffusivity (m^2/s)
B_0	magnetic induction	β	thermal expansion coefficient ($1/\text{K}$)
C	specific heat ($\text{J}/\text{kg K}$)	ϵ	Carman–Kozeny equation constant
C_p	specific heat in constant pressure ($\text{J}/\text{kg K}$)	γ	the ratio of thermal diffusivity
f	nondimensional liquid fraction	$\phi(T)$	liquid fraction
g	gravity (m/s^2)	μ	dynamic viscosity ($\text{kg}/\text{m.s}$)
Ha	Hartmann number	θ	nondimensional temperature
k	thermal conductivity ($\text{W}/\text{m K}$)	ρ	density (kg/m^3)
L	latent heat of fusion (J/kg)	σ	electrical conductivity
L_x	length in x -direction (m)	ν	kinematic viscosity (m^2/s)
L_y	length in y -direction (m)	$\xi(x,y)$	horizontal and vertical coordinate in a unit square
N	total number of grid nodes	ΔT	mushy-zone temperature range (K)
\overline{Nu}	average Nusselt number	Subscripts	
P	pressure (Pa)	c	cold
Pr	Prandtl number	F	fusion
Ra	Rayleigh number	h	hot
$S(T)$	Carman–Kozeny equation (source term)	p	interface position
Ste	Stefan number	l	liquid phase
T	temperature (K)	k	node number
t	time (s)	R	ratio
T_f	melting temperature (K)	i	residual number
u	velocity in the x -direction (m/s)	s	solid phase

Considering the finite-volume approach and temperature-transforming model, a new method for the correction of the solid velocity with an explicit update for buoyancy force and melting front is proposed. Chamkha et al. [7] studied melting, radiation, heat generation, and adsorption impacts on mixed convection from a vertical plate assuming non-Newtonian fluid saturated in non-Darcy porous medium. Tiwari et al. [8], considering a two-dimensional model, numerically studied the thermal characteristics of a fin heat pipe-assisted latent heat thermal energy storage system. In order to optimize the design of solar passive walls including PCMs heated from a vertical wall of a rectangular cavity, Joulin et al. [9] tried to formulate, implement, and validate a numerical method. Khodadadi and Hosseinzadeh [10] enhanced the functionality of the PCMs through dispersion of nanoparticles. They improved the thermal conductivity of the base materials proposing nanoparticle-enhanced phase change materials (NEPCM). Moreover, the effects of surface waviness and nanoparticle dispersion on solidification of Cu–water nanofluid into a vertical cavity were studied by Kashani et al. [11]. Considering nanofluids, Zhang et al. [12] have studied the unsteady natural convection heat transfer of nanofluids in an annulus enclosure.

In some manufacturing and metallurgical processes, natural convection heat transfer is not appropriate due to the fact that such a process should be meticulously controlled. Therefore, investigators obviate this problem utilizing natural convection of electrically conducting fluids in a magnetic field. Proper research and thorough comprehension of the heat transfer and momentum in such processes is crucial for better control which results in enhancing the quality of products. Due to very important controlling advantages of MHD flows, the free convection heat transfer of nanofluids in a cavity [13] and a channel [14] in the presence of a magnetic field has been studied very recently. Xu et al. [15] implemented an experimental study of thermally induced convection of molten gallium subject to a uniform magnetic field which is assumed to be parallel to the temperature gradient. The influence of magnetic field on natural convection flow in a square enclosure filled with liquid gallium, considering heated side walls, is studied by Sathiyamoorthy and Chamkha [16]. Jena et al. [17] investigated the magnetoconvection of molten gallium by applying a vertical magnetic field through a center of cuboid opposite to the direction of gravity. Feng et al. [18] have addressed MHD phase change heat transfer

of gallium in a cavity heated from below. They have analyzed the effect of magnetic field and the inclination angle of the magnetic field on the melting process of gallium. They reported that the magnetic field with an inclination angle has a significant impact on the flow and heat transfer in the melting process.

To the best of the authors' knowledge, the effect of the presence of a magnetic field on a phase change process of a differentially heated tilted cavity has not been addressed yet. The motivation behind the present work is to study the melting of an electrically conductive substance in the presence of a magnetic field in an inclined cavity. The fundamental results of the present study could be of interest in future modeling and control of the functionality of the MHD phase change processes in metallurgical processes and thermal systems.

2. Geometric and mathematical models

2.1. Physics of the problem

Consider a rectangular cavity with the width L_x and height L_y . A schematic view of the physical model is represented in Figure 1. The rectangular cavity is filled with an electrically conductive frozen substance (solid) such as gallium or an electrolyte inside an inclined rectangular enclosure. It is assumed that the temperatures of the left and right walls are T_h , where $T_h > T_f$ in which T_f is the melting temperature of the substance. The bottom and top walls are insulated and the substance inside the cavity is initially at the uniform temperature of T_f . A uniform magnetic field with magnitude B_0 is applied normal to the vertical walls as shown in Figure 1.

2.2. Governing equations

The enclosure walls are considered to be rigid, conducting, and impermeable. Moreover, the temperature differences are assumed to be small, and hence, the thermophysical properties in each phase are constant, and the Boussinesq approximation is applicable for considering the density changes in the

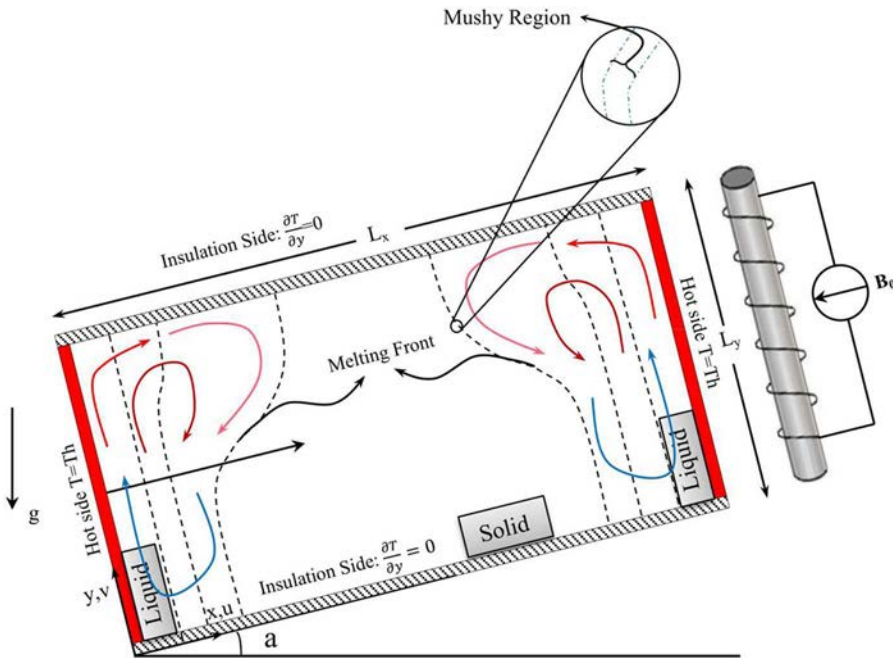


Figure 1. Schematic diagram of a physical model.

liquid phase. However, the thermophysical changes due to phase change is taken into account as the density, heat capacity, and thermal conductivity for the solid and liquid phases of a substance could be different. It is also assumed that Joule heating effects as well as viscous dissipation effects and radiation effects are negligible. The induced magnetic field due to the induced current in the cavity is neglected as the magnetic Reynolds number is small. Considering the above assumptions, the conservation equations for mass, momentum, temperature, and the electric transfer are written as [1, 8, 19]

Continuity

$$\nabla \cdot u = 0 \quad (1)$$

Momentum

$$\rho \left(\frac{\partial u}{\partial t} + (u \cdot \nabla)u \right) = -\nabla P + \nabla \cdot (\mu(\varphi)\nabla u) + F \quad (2)$$

Energy

$$\frac{\partial T}{\partial t} + (u \cdot \nabla)T = \nabla(\alpha(\varphi)\nabla T) - \frac{L}{c_p} \frac{\partial \varphi(T)}{\partial t} \quad (3)$$

where the F term in Eq. (2) is the volume force that is explained as follows:

$$F = F_L + F_B + S(T) \cdot u \quad (4)$$

The term F in Eq. (2) is the result of three sub-terms, the magnetic field (F_L) force, the buoyancy force (F_B), and the Carman–Kozeny model ($S(T)$). Here, φ is the liquid volume fraction. F_L is the effect of the magnetic field that is entered in the momentum equations in the form of the Lorentz volume force as [20]

$$F_L = J \times B \quad (5)$$

where J and B are also expressed as follows [19]:

$$J = \sigma(-\nabla\phi + V \times B) \quad (6a)$$

$$\nabla^2\phi = B \cdot \omega, \quad \omega = \nabla \times V \quad (6b)$$

where u , B , V , ω , and J are the velocity, the magnetic, the vorticity, and the voltage fields, respectively. The variables of P , T , ϕ , and φ denote the pressure, the temperature, the electric potential, and the volume fraction of the liquid phase, respectively. Here, t is time and g is the vector of gravitational acceleration constant. In addition, α is the thermal diffusivity, L is the latent heat of fusion, C_p is the heat capacity at constant pressure, ρ is the density, β is the thermal expansion coefficient, ν is the kinematic viscosity, and σ is the electrical conductivity. Subscripts l and s denote the liquid and solid phases, respectively. In Eq. (4), the term $S(T) \cdot u$ indicates a source term for forcing the fluid velocity to zero in solid phase which will be discussed in more detail later.

Sreenivasan et al. [21] discussed the effect of magnetic field on the flow motion and concluded that for the case of two-dimensional steady flow and where the magnetic field lies in the plane of motion the term $B \cdot \omega$ is zero, and hence, the governing Eq. (6b) reduces to $\nabla^2\phi = 0$. Taking into account that the enclosure walls are perfectly electrically conductive, they could provide a very low resistance guide path for the induced current. Therefore, it can be concluded that the electric field vanishes everywhere in the cavity [16]. Invoking these conditions, the term $J \times B$ in the momentum equation reduces to σB^2 [19].

The term F_B in Eq. (4) is the buoyancy force that leads to convection heat transfer in the liquid (molten) and is expressed by Boussinesq approximation as follows:

$$\vec{F} = \rho\beta\vec{g}(T - T_f) \quad (7)$$

Finally, the term $S(T)$ in Eq. (4) is the body force effect of the Carman–Kozeny model that expresses the effect of damping in the mushy region. In the Carman–Kozeny model, it is assumed the mushy region is a porous medium, in which by moving from the liquid toward the solid part, the porosity and the permeability of the medium gets very low, and hence, the velocity of the fluid tends to zero. The term of $S(T)$ in the momentum equation is defined as [8]

$$S(T) = -A_{\text{mush}} \frac{(1 - \varphi(T))^2}{\varphi(T)^3 + \varepsilon} \quad (8)$$

where φ is a function of temperature defining the solid and liquid regions by:

$$\varphi(T) = \begin{cases} 0 & T < T_f \\ \frac{T - T_f}{\Delta T} & T_f < T < T_f + \frac{\Delta T}{2} \\ 1 & T > T_f + \Delta T \end{cases} \quad (9)$$

In the present study, the viscosity is also controlled in the mushy region using the following relation:

$$\mu(\varphi) = \mu_l(1 + A_{\text{mush}}(1 - \varphi)) \quad (10a)$$

Control of viscosity in the mushy region, using Eq. (10), assists the uniformity of the velocity and pressure fields in the domain of the solution. It also helps the velocity field to remain zero at the solid parts of the domain. The thermal diffusivity in the liquid, mushy, and solid region is assumed as a linear function of the volume fraction of the liquid as

$$\alpha(\varphi) = \varphi\alpha_l + \alpha_s(1 - \varphi) \quad (10b)$$

Now, the governing equations for mass, momentum, and thermal energy represented here in dimensional Cartesian coordinates x, y can be written as follows:

Continuity

$$\frac{\partial u}{\partial x} + \frac{\partial v}{\partial y} = 0 \quad (11)$$

Momentum in x -direction

$$\rho \left(\frac{\partial u}{\partial t} + u \frac{\partial u}{\partial x} + v \frac{\partial u}{\partial y} \right) = -\frac{\partial p}{\partial x} + \left(\frac{\partial}{\partial x} \left(\mu(\varphi) \frac{\partial u}{\partial x} \right) + \frac{\partial}{\partial y} \left(\mu(\varphi) \frac{\partial u}{\partial y} \right) \right) + \rho \vec{g} \beta (T - T_f) \sin a + S(T) \cdot u \quad (12)$$

Momentum in y -direction

$$\rho \left(\frac{\partial v}{\partial t} + u \frac{\partial v}{\partial x} + v \frac{\partial v}{\partial y} \right) = -\frac{\partial p}{\partial y} + \left(\frac{\partial}{\partial x} \left(\mu(\varphi) \frac{\partial v}{\partial x} \right) + \frac{\partial}{\partial y} \left(\mu(\varphi) \frac{\partial v}{\partial y} \right) \right) + \rho \vec{g} \beta (T - T_f) \cos a - (\sigma B_0^2) \cdot v + S(T) \cdot v \quad (13)$$

Energy

$$\frac{\partial T}{\partial t} + u \frac{\partial T}{\partial x} + v \frac{\partial T}{\partial y} = \left(\frac{\partial}{\partial x} \left(\alpha(\varphi) \frac{\partial T}{\partial x} \right) + \frac{\partial}{\partial y} \left(\alpha(\varphi) \frac{\partial T}{\partial y} \right) \right) + \frac{L}{C_p} \frac{\partial \varphi(T)}{\partial t} \quad (14)$$

Based on the problem description, the boundary conditions are written as:

$$\text{Heated wall} \quad x = 0, L_x \quad y = y : \quad u = 0, \quad v = 0, \quad T = T_h \quad (15a)$$

$$\text{Top wall} \quad x = x, \quad y = L_y : \quad u = 0, \quad v = 0, \quad \frac{\partial T}{\partial y} = 0 \quad (15b)$$

$$\text{Bottom wall} \quad x = x, \quad y = 0 : \quad u = 0, \quad v = 0, \quad \frac{\partial T}{\partial y} = 0 \quad (15c)$$

where L_x and L_y are the width and height of the enclosure, respectively. At the beginning, the cavity is filled with the solid phase at the fusion temperature of T_f .

It is appropriate to express Eqs. (11)–(14) in nondimensional form using the following dimensionless variables as:

$$X = \frac{x}{L_y}, \quad Y = \frac{y}{L_y}, \quad U = \frac{uL_y}{\alpha_l}, \quad V = \frac{vL_y}{\alpha_l}, \quad \theta = \frac{T - T_f}{T_h - T_f} \quad (16a)$$

$$\text{Fo} = \frac{t\alpha_l}{L_y^2}, \quad S(T) = \frac{S(T)L_y^2}{\rho\alpha_l}, \quad \mu_r = \frac{\mu(\varphi)}{\mu_l}, \quad \alpha_r = \frac{\alpha(\varphi)}{\alpha_l}, \quad P = \frac{pL_y^2}{\rho\alpha_l^2}, \quad \text{AR} = \frac{L_y}{L_x} \quad (16b)$$

Invoking the nondimensional variables, the corresponding nondimensional form of the governing Eqs. (11)–(14) is obtained as

Continuity:

$$\frac{\partial U}{\partial X} + \frac{\partial V}{\partial Y} = 0 \quad (17)$$

Momentum in x -direction:

$$\frac{\partial U}{\partial \text{Fo}} + U \frac{\partial U}{\partial X} + V \frac{\partial U}{\partial Y} = -\frac{\partial p}{\partial X} + \text{Pr} \left(\frac{\partial}{\partial X} \left(\mu_r \frac{\partial U}{\partial X} \right) + \frac{\partial}{\partial Y} \left(\mu_r \frac{\partial U}{\partial Y} \right) \right) + \text{Ra Pr } \theta \sin a + S(T) \cdot U \quad (18)$$

Momentum in y -direction:

$$\begin{aligned} \frac{\partial V}{\partial \text{Fo}} + U \frac{\partial V}{\partial X} + V \frac{\partial V}{\partial Y} = & -\frac{\partial p}{\partial Y} + \text{Pr} \left(\frac{\partial}{\partial X} \left(\mu_r \frac{\partial V}{\partial X} \right) + \frac{\partial}{\partial Y} \left(\mu_r \frac{\partial V}{\partial Y} \right) \right) \\ & + \text{Ra Pr } \theta \cos a - (\text{Ha})^2 \text{Pr} \cdot V + S(T) \cdot V \end{aligned} \quad (19)$$

Energy:

$$\frac{\partial \theta}{\partial \text{Fo}} + U \frac{\partial \theta}{\partial X} + V \frac{\partial \theta}{\partial Y} = \left(\frac{\partial}{\partial X} \left(\alpha_r \frac{\partial \theta}{\partial X} \right) + \frac{\partial}{\partial Y} \left(\alpha_r \frac{\partial \theta}{\partial Y} \right) \right) - \frac{1}{\text{Ste}} \frac{\partial f}{\partial F_0} \quad (20)$$

The relevant dimensionless parameters are then:

$$\text{Ra} = \frac{\rho g \beta L_y^3 (T_h - T_f)}{\mu_l \alpha_l} \quad (21)$$

$$\text{Ste} = \frac{c_l (T_h - T_f)}{L} \quad (22)$$

$$\text{Pr} = \frac{c_l \mu_l}{k_l} \quad (23)$$

$$\text{Ha} = B_0 L_y \sqrt{\frac{\sigma}{\rho \nu}} \quad (24)$$

Following Eq. (16), the nondimensional form of the viscosity and thermal diffusivity equations, Eqs. (10a) and (10b) can be evaluated as follows:

$$\mu_r = (1 + A_{\text{mush}}(1 - \varphi)) \quad (25a)$$

$$\alpha_r = \left(1 + \frac{\alpha_s}{\alpha_l} (1 - \varphi) \right) \quad (25b)$$

where Ra is the Rayleigh number, Ste is the Stefan number, Pr is the Prandtl number, and Ha is the Hartmann number. By using the variables in Eq. (16), the nondimensional boundary conditions are

$$\text{Heated wall} \quad X = 0, 1 : \quad U = 0, \quad V = 0, \quad \theta_h = 1 \quad (26a)$$

$$\text{Top wall} \quad Y = AR : \quad U = 0, \quad V = 0, \quad \frac{\partial \theta}{\partial Y} = 0 \quad (26b)$$

$$\text{Bottom wall} \quad Y = 0 : \quad U = 0, \quad V = 0, \quad \frac{\partial \theta}{\partial Y} = 0 \quad (26c)$$

The melt volume fraction as a function of θ is written as:

$$\varphi(\theta) = \begin{cases} 0 & \theta < 0 \\ \frac{\theta}{\Delta\theta} & 0 < \theta < \Delta\theta \\ 1 & \theta > \Delta\theta \end{cases} \quad (27)$$

where $\Delta\theta = \frac{\Delta T}{T_h - T_f}$. The initial temperature in nondimensional form is evaluated as $\theta = 0$ in the cavity.

3. Method of solution and validation

The system of partial differential Eqs. (17)–(20) along with the boundary conditions, Eq. (26), are transformed into weak form and solved numerically utilizing the Galerkin finite element method [22]. The continuity Eq. (17) is employed as a constraint to satisfy the mass conservation by the control of the pressure distribution using the mass conservation. Thus, the following constraint equation for continuity equation is utilized as a penalty parameter (χ) in the momentum equations as described by Reference [22]. Therefore, the pressure is written as

$$P = \chi \left(\frac{\partial U}{\partial X} + \frac{\partial V}{\partial Y} \right) \quad (28)$$

where χ is the penalty number, which is a large value. Invoking Eq. (28), the momentum Eqs. (18) and (19) are obtained as

$$\begin{aligned} \frac{\partial U}{\partial Fo} + U \frac{\partial U}{\partial X} + V \frac{\partial U}{\partial Y} = & - \frac{\partial}{\partial X} \left(\chi \left(\frac{\partial U}{\partial X} + \frac{\partial V}{\partial Y} \right) \right) + Pr \left(\frac{\partial}{\partial X} \left(\mu_r \frac{\partial U}{\partial X} \right) + \frac{\partial}{\partial Y} \left(\mu_r \frac{\partial U}{\partial Y} \right) \right) \\ & + Ra \, Pr \, \theta \sin a + S(T) \cdot U \end{aligned} \quad (29)$$

$$\begin{aligned} \frac{\partial V}{\partial Fo} + U \frac{\partial V}{\partial X} + V \frac{\partial V}{\partial Y} = & - \frac{\partial}{\partial Y} \left(\chi \left(\frac{\partial U}{\partial X} + \frac{\partial V}{\partial Y} \right) \right) + Pr \left(\frac{\partial}{\partial X} \left(\mu_r \frac{\partial V}{\partial X} \right) + \frac{\partial}{\partial Y} \left(\mu_r \frac{\partial V}{\partial Y} \right) \right) \\ & + Ra \, Pr \, \theta \cos a - (Ha)^2 \, Pr \cdot V + S(T) \cdot V \end{aligned} \quad (30)$$

Thus, in the above equations, the continuity Eq. (17) is satisfied for very large values of the penalty parameter ($\chi = 10^7$) [22]. Now, the velocities (U and V) as well as the temperature, θ , are expanded invoking a basis set $\{\xi_k\}_{k=1}^N$ in the domain interval of $-0.5 < X < 0.5$ and $0 < Y < 1$ as

$$U \approx \sum_{k=1}^N U_k \zeta(X, Y), \quad V \approx \sum_{k=1}^N V_k \zeta(X, Y), \quad \theta \approx \sum_{k=1}^N \theta_k \zeta(X, Y) \quad (31)$$

Here it should be noted that the basis function ζ for all of the three variables is the same. Therefore, the total number of nodes is $N = 3$. Invoking the introduced basis functions introduced

in Eq. (31), the nonlinear residual equations (R_i^N) of the governing equations, Eqs. (17)–(20), are derived as follows:

$$\begin{aligned}
 R_i^1 = & \sum_{k=1}^N U_k \int_{\Omega} \frac{\partial \xi_K}{\partial F_0} \xi_i dXdY \\
 & + \sum_{k=1}^N U_k \int_{\Omega} \left[\left(\sum_{k=1}^N U_k \zeta_k \right) \frac{\partial \zeta_k}{\partial X} + \left(\sum_{k=1}^N V_k \zeta_k \right) \frac{\partial \zeta_k}{\partial Y} \right] \xi_i dXdY \\
 & + \sum_{k=1}^N U_k \int_{\Omega} \frac{\partial \xi_i}{\partial X} \left[(\chi) \frac{\partial \xi_K}{\partial X} dXdY \right] + \sum_{k=1}^N V_k \int_{\Omega} \frac{\partial \xi_i}{\partial X} \left[(\chi) \frac{\partial \xi_K}{\partial Y} dXdY \right] \quad (32)
 \end{aligned}$$

$$\begin{aligned}
 & + \Pr \left[\sum_{k=1}^N U_k \int_{\Omega} \frac{\partial \xi_i}{\partial X} \left(\mu_r \frac{\partial \xi_K}{\partial X} dXdY \right) + \sum_{k=1}^N U_k \int_{\Omega} \frac{\partial \xi_i}{\partial Y} \left(\mu_r \frac{\partial \xi_K}{\partial Y} dXdY \right) \right] \\
 & + \text{Ra} \Pr \left[\int_{\Omega} \left(\sum_{k=1}^N \theta_k \zeta_k \right) \xi_i dXdY \right] \sin a + S(T) \sum_{k=1}^N \int_{\Omega} \left(\sum_{k=1}^N (U_k \zeta_k) \xi_i \right) dXdY \\
 R_i^2 = & \sum_{k=1}^N V_k \int_{\Omega} \frac{\partial \xi_K}{\partial F_0} \xi_i dXdY \\
 & + \sum_{k=1}^N V_k \int_{\Omega} \left[\left(\sum_{k=1}^N U_k \zeta_k \right) \frac{\partial \zeta_k}{\partial X} + \left(\sum_{k=1}^N V_k \zeta_k \right) \frac{\partial \zeta_k}{\partial Y} \right] \xi_i dXdY \\
 & + \sum_{k=1}^N U_k \int_{\Omega} \frac{\partial \xi_i}{\partial Y} \left[(\chi) \frac{\partial \xi_K}{\partial X} dXdY \right] + \sum_{k=1}^N V_k \int_{\Omega} \frac{\partial \xi_i}{\partial Y} \left[(\chi) \frac{\partial \xi_K}{\partial Y} dXdY \right] \quad (33) \\
 & + \Pr \left[\sum_{k=1}^N V_k \int_{\Omega} \frac{\partial \xi_i}{\partial X} \left(\mu_r \frac{\partial \xi_K}{\partial X} dXdY \right) + \sum_{k=1}^N V_k \int_{\Omega} \frac{\partial \xi_i}{\partial Y} \left(\mu_r \frac{\partial \xi_K}{\partial Y} dXdY \right) \right] \\
 & + \text{Ra} \Pr \left[\int_{\Omega} \left(\sum_{k=1}^N \theta_k \zeta_k \right) \xi_i dXdY \right] \cos a \\
 & + (\text{Ha})^2 \Pr \sum_{k=1}^N \int_{\Omega} \left(\sum_{k=1}^N V_k \zeta_k \right) \xi_i dXdY + S(T) \sum_{k=1}^N \int_{\Omega} \left(\sum_{k=1}^N (V_k \zeta_k) \xi_i \right) dXdY
 \end{aligned}$$

$$\begin{aligned}
 R_i^3 = & \sum_{k=1}^N \theta_k \int_{\Omega} \frac{\partial \xi_K}{\partial F_0} \xi_i dXdY \\
 & + \sum_{k=1}^N \theta_k \int_{\Omega} \left[\left(\sum_{k=1}^N U_k \zeta_k \right) \frac{\partial \zeta_k}{\partial X} + \left(\sum_{k=1}^N V_k \zeta_k \right) \frac{\partial \zeta_k}{\partial Y} \right] \xi_i dXdY \quad (34) \\
 & \left[\sum_{k=1}^N \theta_k \int_{\Omega} \frac{\partial \xi_i}{\partial X} \left(a_r \frac{\partial \xi_K}{\partial X} dXdY \right) + \sum_{k=1}^N \theta_k \int_{\Omega} \frac{\partial \xi_i}{\partial Y} \left(a_r \frac{\partial \xi_K}{\partial Y} dXdY \right) \right] \\
 & + \frac{1}{\text{Ste}} \sum_{k=1}^N f_k \int_{\Omega} \frac{\partial \xi_K}{\partial F_0} \xi_i dXdY
 \end{aligned}$$

In order to numerically evaluate integral terms, the bi-quadratic functions with three-point Gaussian quadrature are employed. Then, the Newton–Raphson method is employed to evaluate the coefficients of the expansions, that is, U_k , V_k , and θ_k , in the nonlinear residual Eqs. (32)–(34). More details about the solution procedure can be found in the excellent studies by Reddy [22] and Basak et al. [23, 24]. In the present study, a non-uniform grid is utilized. The grid points are symmetrically clustered next to the vertical and horizontal walls with the ratio of 1.05. The zero values

for the initial velocities and temperature are adopted. Commencing the solution from the initial values, the system of residual equations are solved iteratively and the calculations are repeated until the residuals for the field variables, that is, velocities and temperature become small (10^{-7} or lower). The solution procedure, in the form of an in-house computational fluid dynamics (CFD) code, has been validated successfully against the results available in the literature including the studies of References [1, 3, 25].

3.1. Grid check

In order to check the grid independency of the solution, the calculations are repeated for several grid sizes in the case of $Pr = 0.0216$, $Ra = 2.1 \times 10^5$, $Ste = 0.039$, $A_{mush} = 1.6 \times 10^6$. Table 1 indicates the required time for simulation of approximately 90% of melting for various grid sizes. The calculations are performed using a supercomputer with 40 GB of memory and 20 CPU cores each of 2.2 GHz. The liquid fraction for different grid sizes is also depicted in Figure 2. The results of Figure 2 indicate that the grid size of 150×150 can provide acceptable accuracy. Hence, the results of the present study are carried out using the grid size 150×150 .

3.2. Validation of the results

To check the precision of the solution, several investigations have been performed. As the first case, the results of the present study are compared with the experimental results of Gau and Viskanta [25] and the numerical results available in literature for a rectangular cavity with aspect ratio (height/width) of 0.714. In the experiment of Gau and Viskanta [25], the left wall is hot, while the top and bottom walls are insulated.

Gau and Viskanta [25] have evaluated the melting interface using the pour-out method and the probing method. The evaluated melting interface for this problem is also numerically addressed by Kashani et al. [11], Khodadadi and Hosseinzadeh [10], Brent et al. [2], Joulin, et al. [9], Viswanta and Jaluria [26], and Dessai and Vafai [27]. The summary of the available numerical results are plotted in Figures 3a and 3b. As seen, the results of the present study are in reasonable agreement with the available experimental and numerical results. In the case of $Fo = 3.48$, the results are somehow different from the experiment but in agreement with the numerical results. The previous authors have concluded that the difference between the numerical and experimental results in this case could be due to the method of evaluating the melting interface in the experiment of Gau and Viskanta [25]. The authors have measured the melting interface mechanically using a manual mechanical probe. For high values of Fo , the solid-liquid interface of melting could be unstable, and hence, distinguishing the precise shape of the interface is hard.

As another validation, the results of the present finite element code are compared with the benchmark study of Bertrand et al. [1] when $Ra = 1 \times 10^7$, $Pr = 50$, $Ha = 0$, and $\alpha_s/\alpha_l = 1$. In the study of Bertrand et al. [1] as a benchmark study, different authors have reported the results of the melting interface for a square cavity. The results are shown in Figure 4. As seen, there is a good agreement between the results of the present study and the results available in the literature.

Also, as another comparison, the results of the present study are compared with the experimental results reported by Kumar et al. [3] for melting of lead. Kumar et al. [3] have examined the melting of

Table 1. The required time for grid size independency.

Cases	Grid size	Run time
Case 1	100×100	14 h, 21 min
Case 2	125×125	1 day, 6 h, 12 min
Case 3	150×150	2 day, 1 h, 20 min
Case 4	175×175	2 days, 18 h, 27 min
Case 5	200×200	3 days, 10 h, 48 min

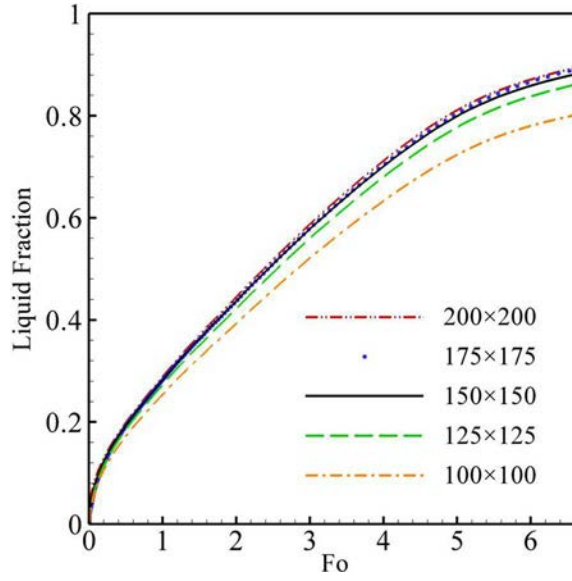


Figure 2. The liquid fraction for various grid sizes.

lead contained in a stainless steel cuboid. In the study of Kumar et al. [3], there was a heater mounted at one of the vertical side walls of the cavity which provided a constant heat flux, while the other walls were insulated. The authors have carried out the photography of solid–liquid interface movement during melting of lead using neutron radiography. The nondimensional parameters of the experimental setup of Kumar et al. [3] are shown in Table 2. Initially, the heater is put on and the temperature increases on both sides. In the experiment of Kumar et al. [3], when melting commenced, the temperature at the right-hand side walls (the heater side) was higher than that of the left-hand side wall. Therefore, a linear temperature distribution was the initial condition for the commencing of the melting process. As Kumar et al. [3] have performed the experiment for the case of constant heat flux, the Rayleigh number, Stefan number, and the Prandtl number are needed to be calculated on the basis of the constant heat flux as $Ste^* = C_p q''_{cond} L_x / (kL)$ and the Rayleigh number based on constant heat flux is given by $Ra^* = g\beta q''_{cond} L_y^4 / (k\alpha\nu)$ and $Ste^* = C_p q''_{cond} L_x^4 / (kL)$. Here, the results of the present study are compared with the experimental results reported by Kumar et al. [3] for a case indicated in Table 3.

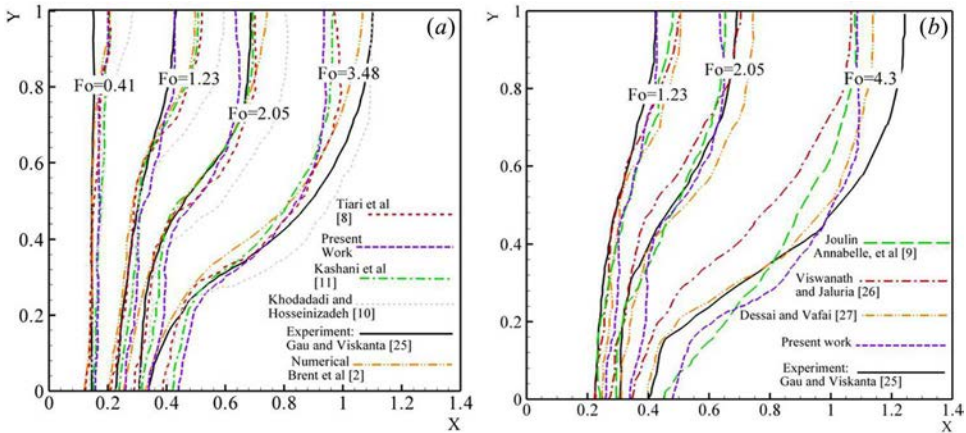


Figure 3. A comparison among the experimental measurement of Gau and Viskanta [25], the numerical results available in literature, and the results of the present study when $\gamma = 1$ and neglecting the magnetic effects (a) and (b): uniformly heated left and cooled right. The bottom and top walls are insulated, $Ra = 6 \times 10^5$, $Pr = 0.0216$.

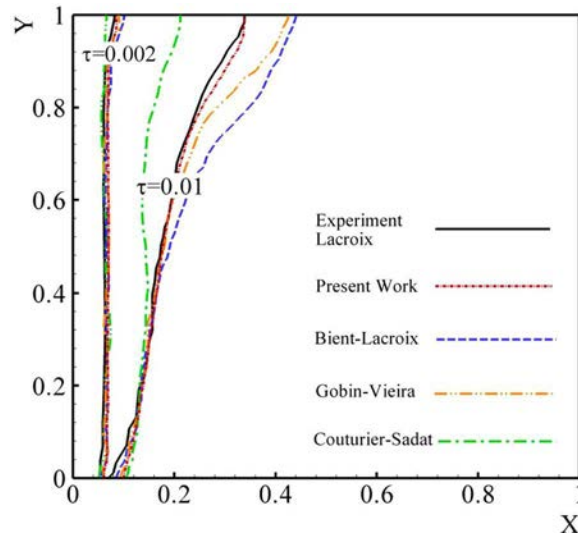


Figure 4. A comparison among the benchmark study of Bertrand et al. [1] and the results of the present study ($\tau = Fo \times Ste$) when (a) $\tau = 6 \times 10^{-3}$; (b) $\tau = 1 \times 10^{-2}$.

Table 2. Input provided for one case in the simulation of Kumar et al. [3].

Heater input (right side)	Stefan number	Prandtl number	Rayleigh number	Hartmann number	Temperature at left side (K)	Temperature at right side (K)
16.3 kW/m ²	0.4	0.0236	1.4×10^7	0	555	599

For the case of magnetohydrodynamic flows, Sathiyamoorthy and Chamkha [19] have studied the effect of the presence of magnetic field effects on natural convection of electrically conducting liquids. In this regard, Sathiyamoorthy and Chamkha [19] have studied the natural convection flow within a square cavity filled with liquid metals subject to a uniform magnetic field, when the bottom and left walls are uniformly (constant temperature) or linearly heated, while the right and top walls are cooled. It should be noted that in the study of Sathiyamoorthy and Chamkha [19], there was no phase change and the cavity is solely filled with the liquid phase. As a comparison, the results of the present study are compared with the results of the study of Sathiyamoorthy and Chamkha [19] by assuming that the cavity is filled with a molten metal for the case of $Ra = 10^5$, $Pr = 0.054$, and two Hartmann numbers of $Ha = 50$ and $Ha = 100$. Figure 5 shows a comparison between the streamlines and isotherms

Table 3. Boundary locations solid–liquid (\times) at different nondimensional times (Fo): A comparison between the result of the benchmark experimental of Kumar et al. [3] and the results of the present study.

y	$Fo = 1.83$		$Fo = 1.47$		$Fo = 1.1$		$Fo = 0.73$	
	Present work	Kumar et al. [3]	Present work	Kumar et al. [3]	Present work	Kumar et al. [3]	Present work	Kumar et al. [3]
0	0.29	0.29	0.22	0.21	0.17	0.12	0.13	0.08
0.1	0.39	0.29	0.26	0.23	0.19	0.15	0.16	0.09
0.2	0.49	0.40	0.33	0.26	0.21	0.18	0.16	0.10
0.3	0.55	0.56	0.39	0.27	0.28	0.23	0.21	0.17
0.4	0.65	0.58	0.43	0.35	0.30	0.24	0.19	0.17
0.5	0.84	0.78	0.59	0.56	0.30	0.29	0.21	0.18
0.6	0.95	0.90	0.71	0.66	0.41	0.37	0.20	0.20
0.7	1	0.98	0.80	0.77	0.52	0.53	0.27	0.27
0.8	1.06	1.01	0.82	0.82	0.58	0.57	0.37	0.37
0.9	1.07	1.03	0.82	0.83	0.57	0.58	0.38	0.40
1	1.07	1.03	0.85	0.85	0.59	0.57	0.38	0.40

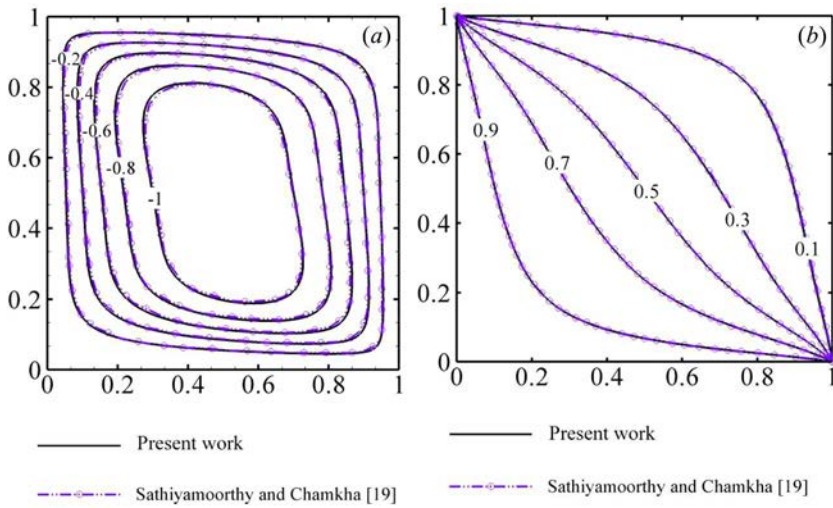


Figure 5. A comparison among the numerical measurements of Sathiyamoorthy and Chamkha [19]: (a) streamlines, (b) isotherms.

reported by Sathiyamoorthy and Chamkha [19] and the results of the present study. Figure 5 indicates good agreement between the results of Sathiyamoorthy and Chamkha [19] and the results of the present study.

As another comparison, the result of the present study for hydromagnetic flows are compared with Al-Mudhaf and Chamkha [28]. In this study, natural convective flow of electrically conducting gallium and germanium liquid metals (only liquid phase) in an inclined rectangular enclosure in the presence of a uniform magnetic field due to a transverse temperature gradient was studied numerically. In the study of Al-Mudhaf and Chamkha [28], the side walls of the cavity were isothermal for which one wall was hot and the other one was cold; the top and bottom were well insulated. In the study of Al-Mudhaf and Chamkha [28], it was assumed that the cavity is filled with solely a liquid phase, and hence, there was no phase change procedure. In this case, the results of the present study are compared with the results of the study of Al-Mudhaf and Chamkha [28] in Table 4. In this case, $Ra=10^5$, $Pr=0.025$, $a=45^\circ$ (where a is enclosure inclination angle).

Table 4. Comparison of the evaluated average Nusselt number \overline{Nu} on the hot wall of the cavity with reference to Al-Mudhaf and Chamkha [28].

Ha	Al-Mudhaf and Chamkha [28]	Present study
30	2.78	2.67
50	1.86	1.81
70	1.43	1.39
100	1.14	1.12

4. Results and discussion

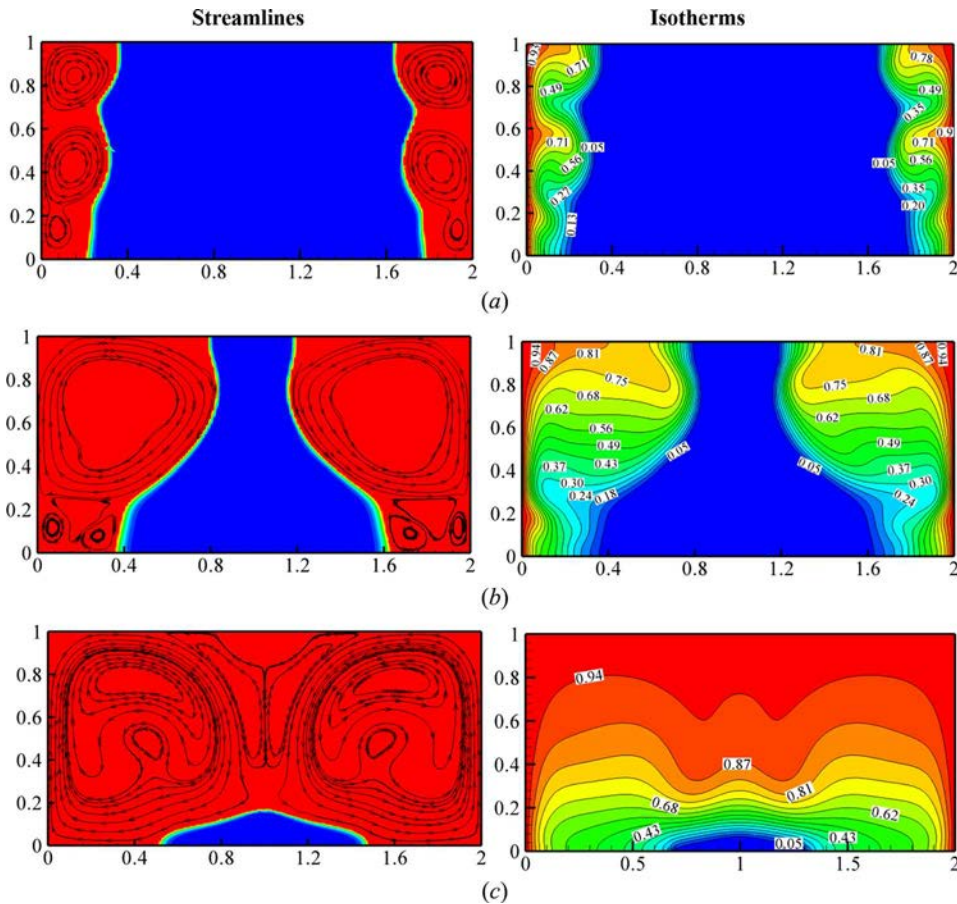
Now, as a case study consider a rectangular cavity with the size of $L_x = 14.4$ cm, $L_y = 7.2$ cm filled with gallium. The temperature at the hot walls is $T_h = 39^\circ\text{C}$. The thermophysical properties of gallium are represented in Table 4. In this case, the corresponding nondimensional parameters are $Pr = 0.0216$, $Ste = 0.044$, $Ra = 1 \times 10^6$, and $\alpha_s/\alpha_l = 1$. These nondimensional parameters are considered as the default nondimensional parameters in this study and the calculations are performed for these set of nondimensional parameters, and otherwise the value of the nondimensional parameter will be stated. The physical properties for pure gallium are obtained and shown in Table 5.

Table 5. Thermophysical properties of pure gallium.

Property	Symbol	Value	Unit
Density (solid/liquid)	ρ	6,093	(kg/m ³)
Thermal expansion coefficient	β	1.2×10^{-4}	(1/K)
Fusion temperature	T_f	302.85	(K)
Thermal conductivity (solid/liquid)	k	32.0	(W/m.K)
Latent heat of fusion	L	80,160	(J/kg)
Specific heat capacity (solid/liquid)	C	381.5	(J/kg.K)
Dynamic viscosity	μ	1.81×10^{-3}	(kg/m.s)

The present study aims to analyze the impact of variation of Ha and inclination angle α on the melting process. In order to investigate the effect of the Hartmann number, the streamlines and isotherms of the melting process, in the case for which the enclosure is horizontal, for various Fourier and Hartmann numbers are presented in Figures 6–8.

As it is shown in Figures 6–8, the rate of the melting process is a decreasing function of the Hartmann number. As the Hartmann number is the ratio of the electromagnetic force to the viscous force, a high value of Ha means that the electromagnetic force is the dominant force compared with the viscous one. Consequently, the magnitude of the viscous force is low and it affects the Gibbs free energy. In other words, the melting process occurs when the Gibbs free energy of the liquid becomes lower than that of the solid for the material and a decrease in viscous flow influences this energy.


Figure 6. Isotherms and streamlines for $Ha = 0$, $a = 0$ when (a) $Fo = 0.7$; (b) $Fo = 2.15$; (c) $Fo = 3.6$.

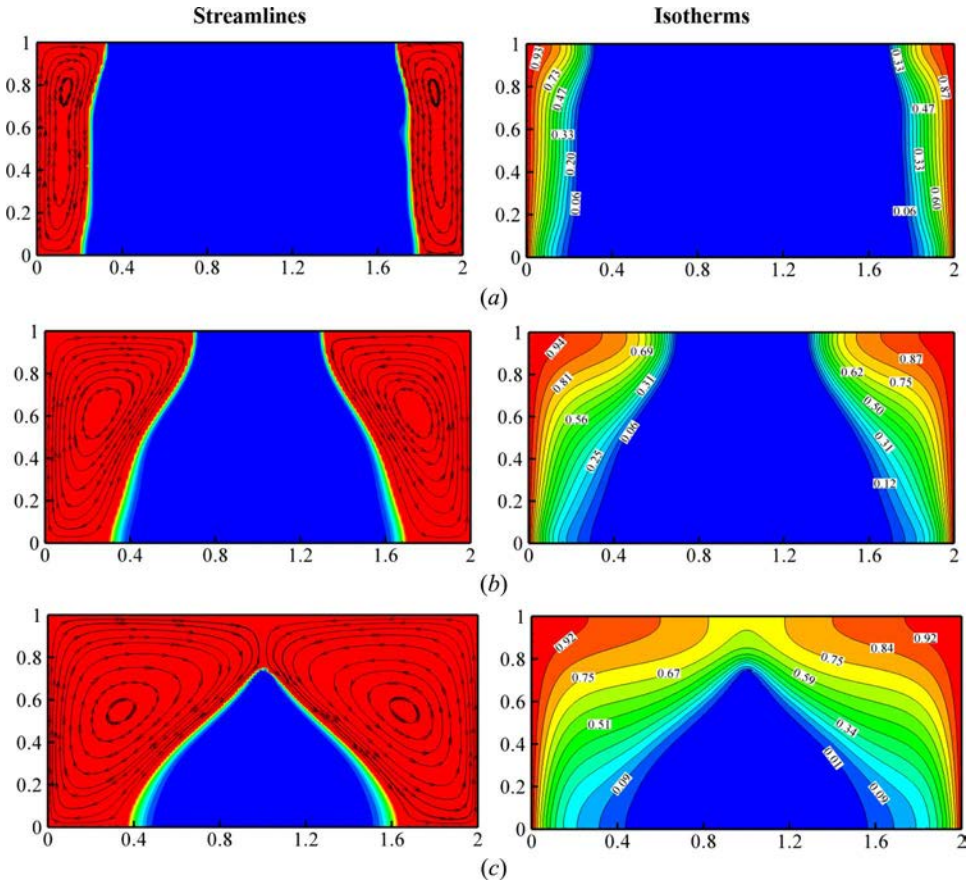


Figure 7. Isotherms and streamlines for $Ha = 100$, $a = 0$ when (a) $Fo = 0.7$; (b) $Fo = 2.15$; (c) $Fo = 3.6$.

To clarify the effect of the Hartmann number on the melting process, the variation of the liquid fraction for different Fourier numbers and Ha is shown in Figure 9.

Based on Figure 9, it is clear that augmentation of Fo leads to an increase in the liquid fraction. Moreover, for low values of Fourier numbers, that is, $Fo < 0.5$, the variation of the Hartmann number does not have significant effect on the liquid fraction. On the other hand, further increase in the Fourier number for Fo greater than 0.5 leads to more difference between liquid fractions. One other point to note is that when the parameter Ha goes up, the liquid fraction magnitude descends. The variation of the melting interface for multifarious Hartmann numbers and inclination angles has been depicted in Figure 10.

According to Figures 10a–10d, the melting process in the inclined enclosure is not symmetric and the progression of melting of the left section, which is placed at the bottom of the right one, is further than the right section. In addition, in the case for which the parameter $Ha = 0$, the melting phenomenon has taken place before the cases corresponding to $Ha = 100$, 200 and the differences between these two cases are much noticeable in the left part compared with the right one. To clarify how the variation of the inclination angle affects the melting interface for different Fourier numbers, Figure 11 is displayed.

In accordance to Figure 11, it is obvious that the effect of alteration of the inclination angle on the melting interface rises as the nondimensional time increases. Moreover, the melting interface is a decreasing function of the angle. As an illustration, when the Fourier number is 3.6, the percentage of the melted material for $a = 0$ is clearly more than the cases corresponding to $a = 30$, 60. Eventually,

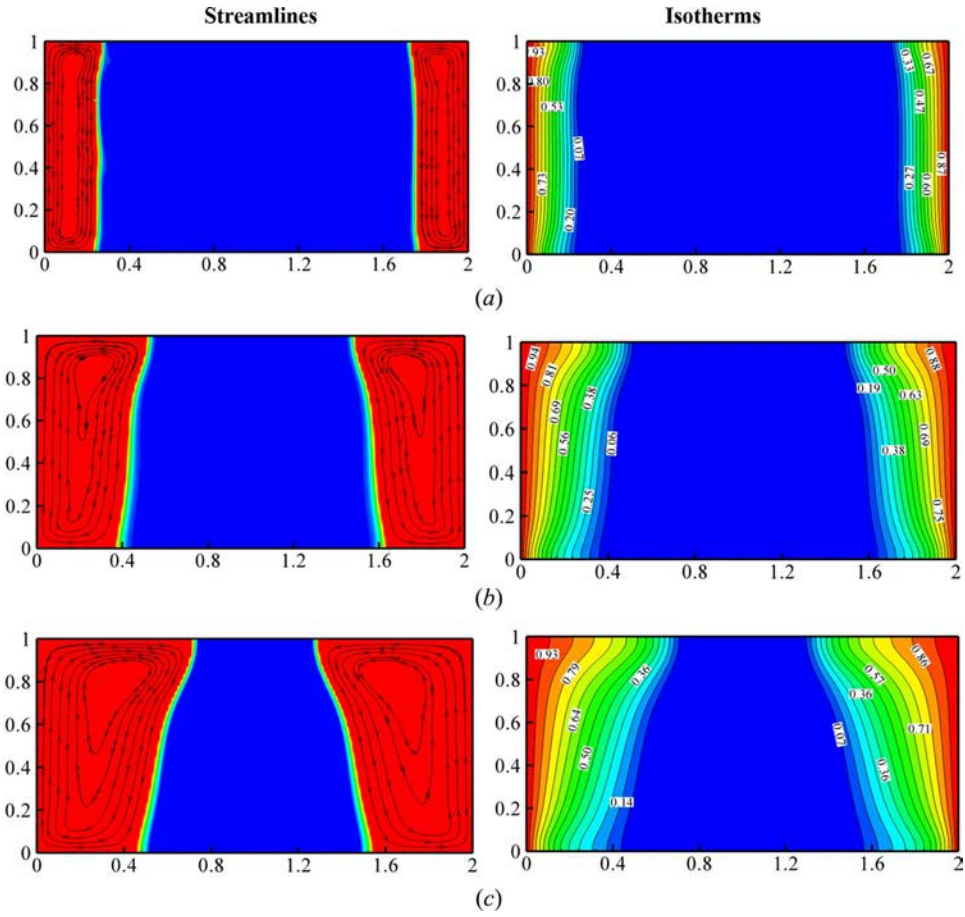


Figure 8. Isotherms and streamlines for $Ha = 200$, $a = 0$ when (a) $Fo = 0.7$; (b) $Fo = 2.15$; (c) $Fo = 3.6$.

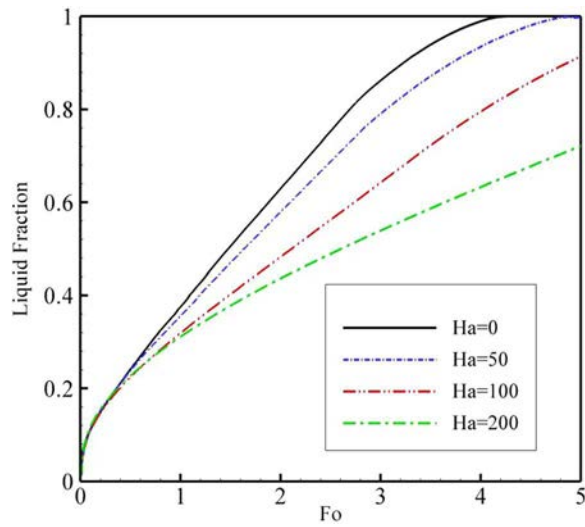


Figure 9. Effect of magnetic induction on liquid fraction without an incline enclosure ($a = 0^\circ$) for various Hartmann number.

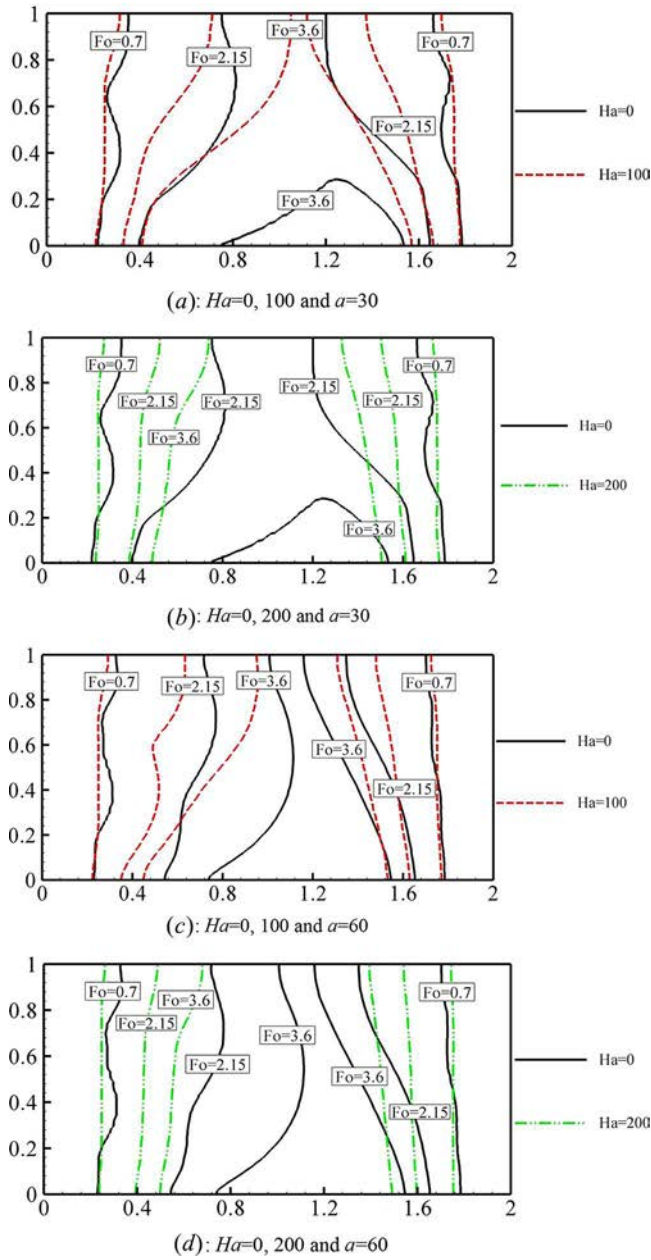


Figure 10. The melting interface for different Hartmann numbers: (a) $Ha = 0, 100$ and $\alpha = 30$; (b) $Ha = 0, 200$ and $\alpha = 30$; (c) $Ha = 0, 100$ and $\alpha = 60$; (d) $Ha = 0, 200$ and $\alpha = 60$.

for more investigation, the impact of changing the inclination angle on the liquid fraction is shown in Figure 12.

As expounded in Figure 12, following the results of Figure 11, any increase in the inclination angle leads to a decrease in the liquid fraction. In other words, changing the value of the inclination angle causes the melting process to occur asymmetrically due to the difference in temperature gradients at the right and left sides of the inclined cavity and consequently, the rate of melting becomes slower.

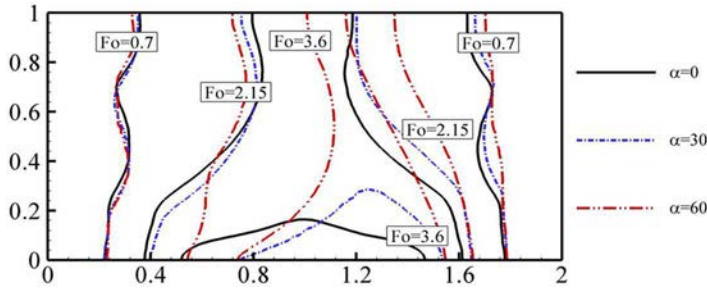


Figure 11. The melting interface for Hartmann number 0 at $\alpha = 0^\circ, 30^\circ, 60^\circ$.

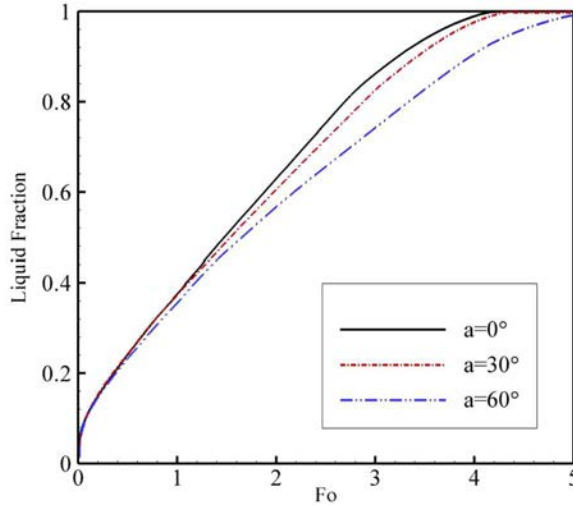


Figure 12. Effect of an inclined enclosure on liquid fraction in Hartmann number 0 ($Ha = 0$).

5. Conclusion

The impact of the magnetic induction and cavity inclination angle on the melting phenomenon of an MHD phase change process is addressed. The left and right vertical walls are maintained at a constant temperature T_h and the bottom and top walls are kept thermally insulated. The effects of crucial parameters such as the Hartmann number and inclination angle of cavity are studied. The results of the present study are compared with the experimental and numerical results available in the literature and found to be in reasonable agreement. The outcomes of the present study can be summarized as follows:

1. The utilized enthalpy–porosity formulation is capable of modeling the phase change phenomenon for a pure substance.
2. The increase of the Hartmann number tends to suppress the convective mechanism and decrease the rate of phase change process.
3. The liquid fraction is a decreasing function of the Stefan number. Furthermore, the augmentation of the inclination angle makes an asymmetric melting, and consequently a decrease in the liquid fraction is predicted.
4. The effect of variation of the Hartmann number (Ha) and the inclination angle (a) on the melting process becomes significant for high values of the Fourier number.

The results of the present study show that the presence of a magnetic field can reduce the advective heat transfer mechanism and induce a more uniform temperature gradient. However, even the presence of a very strong magnetic field is not capable of fully eliminating the effect of the convective heat

transfer mechanism, and the melting interface is not linear. It should be noted that the effects of the cavity inclination angle and the magnetic field strength are addressed in the present study; however, the magnetic inclination angle could also play a significant role on the MHD melting process of PCMs which could be subject of future studies.

Funding

The first and second authors acknowledge the financial support of Dezful Branch, Islamic Azad University, Dezful, Iran. Ghalambaz and Doostanidezfuli are also thankful to National Iranian Drilling Company (NIDC) for the financial support of the present study. The authors are thankful to Sheikh Bahaei National High Performance Computing Center (SBNHPCC) for providing computational resources, supported by the scientific and technological department of the presidential office and Isfahan University of Technology (IUT).

References

- [1] O. Bertrand, B. Binet, H. Combeau, S. Couturier, Y. Delannoy, D. Gobin, M. Lacroix, P. Le Quéré, M. Médale, and J. Mencinger, Melting Driven by Natural Convection A Comparison Exercise: First Results, *Int. J. Therm. Sci.*, vol. 38, no. 1, pp. 5–26, 1999.
- [2] A. Brent, V. Voller, and K. J. Reid, Enthalpy-Porosity Technique for Modeling Convection-Diffusion Phase Change: Application to the Melting of a Pure Metal, *Numer. Heat Transfer Part A*, vol. 13, no. 3, pp. 297–318, 1988.
- [3] L. Kumar, B. Manjunath, R. Patel, S. Markandeya, R. Agrawal, A. Agrawal, Y. Kashyap, P. Sarkar, A. Sinha, and K. Iyer, Experimental Investigations on Melting of Lead in a Cuboid with Constant Heat Flux Boundary Condition Using Thermal Neutron Radiography, *Int. J. Therm. Sci.*, vol. 61, pp. 15–27, 2012.
- [4] Q. Duan, F. Tan, and K. Leong, A Numerical Study of Solidification of n-Hexadecane Based on the Enthalpy Formulation, *J. Mater. Process. Technol.*, vol. 120, no. 1, pp. 249–258, 2002.
- [5] E. Semma, M. El Ganaoui, and R. Bennacer, A. Mohamad, Investigation of Flows in Solidification by Using the Lattice Boltzmann Method, *Int. J. Therm. Sci.*, vol. 47, no. 3, pp. 201–208, 2008.
- [6] S. Wang, A. Faghri, and T. L. Bergman, A Comprehensive Numerical Model for Melting with Natural Convection, *Int. J. Heat Mass Transfer*, vol. 53, no. 9, pp. 1986–2000, 2010.
- [7] A. J. Chamkha, S. E. Ahmed, and A. S. Aloraier, Melting and Radiation Effects on Mixed Convection from a Vertical Surface Embedded in a Non-Newtonian Fluid Saturated Non-Darcy Porous Medium for Aiding and Opposing Eternal Flows, *Int. J. Phys. Sci.*, vol. 5, no. 7, pp. 1212–1224, 2010.
- [8] S. Tiwari, S. Qiu, and M. Mahdavi, Numerical Study of Finned Heat Pipe-Assisted Thermal Energy Storage System with High Temperature Phase Change Material, *Energy Convers. Manage.*, vol. 89, pp. 833–842, 2015.
- [9] A. Joulin, Z. Younsi, L. Zalewski, D. R. Rousse, and S. Lassue, A Numerical Study of the Melting of Phase Change Material Heated from a Vertical Wall of a Rectangular Enclosure, *Int. J. Comput. Fluid Dyn.*, vol. 23, no. 7, pp. 553–566, 2009.
- [10] J. Khodadadi and S. Hosseinzadeh, Nanoparticle-Enhanced Phase Change Materials (NEPCM) with Great Potential for Improved Thermal Energy Storage, *Int. Commun. Heat Mass Transfer*, vol. 34, no. 5, pp. 534–543, 2007.
- [11] S. Kashani, A. Ranjbar, M. Abdollahzadeh, and S. Sebt, Solidification of Nano-Enhanced Phase Change Material (NEPCM) in a Wavy Cavity, *Heat Mass Transfer*, vol. 48, no. 7, pp. 1155–1166, 2012.
- [12] C. Zhang, L. Zheng, Y. Jiang, and X. Zhang, Unsteady Natural Convection Heat Transfer of Nanofluid in an Annulus with a Sinusoidally Heated Source, *Numer. Heat Transfer. Part A*, vol. 69, no. 1, pp. 97–108, 2016.
- [13] M. Sheikholeslami and A. J. Chamkha, Flow and Convective Heat Transfer of a Ferro-Nanofluid in a Double-Sided Lid-Driven Cavity with a Wavy Wall in the Presence of a Variable Magnetic Field, *Numer. Heat Transfer Part A*, vol. 69, no. 10, pp. 1186–1200, 2016.
- [14] M. Sheikholeslami, M. Azimi, and D. D. Ganji, Application of Differential Transformation Method for Nanofluid Flow in a Semi-Permeable Channel Considering Magnetic Field Effect, *Int. J. Comput. Methods Eng. Sci. Mech.*, vol. 16, no. 4, pp. 246–255, 2015.
- [15] B. Xu, B. Li, and D. Stock, An Experimental Study of Thermally Induced Convection of Molten Gallium in Magnetic Fields, *Int. J. Heat Mass Transfer*, vol. 49, no. 13, pp. 2009–2019, 2006.
- [16] M. Sathiyamoorthy and A. Chamkha, Effect of Magnetic Field on Natural Convection Flow in a Liquid Gallium Filled Square Cavity for Linearly Heated Side Wall (s), *Int. J. Therm. Sci.*, vol. 49, no. 9, pp. 1856–1865, 2010.
- [17] S. K. Jena, V. K. R. Yettella, C. P. R. Sandeep, S. K. Mahapatra, and A. J. Chamkha, Three-Dimensional Rayleigh-Bénard Convection of Molten Gallium in a Rotating Cuboid Under the Influence of a Vertical Magnetic Field, *Int. J. Heat Mass Transfer*, vol. 78, pp. 341–353, 2014.

- [18] Y. Feng, H. Li, L. Li, F. Zhan, Investigation of the Effect of Magnetic Field on Melting of Solid Gallium in a Bottom-Heated Rectangular Cavity Using the Lattice Boltzmann Method, *Numer. Heat Transfer Part A*, vol. 69, pp. 1263–1279, 2016.
- [19] M. Sathiyamoorthy and A. J. Chamkha, Natural Convection Flow Under Magnetic Field in a Square Cavity for Uniformly (or) Linearly Heated Adjacent Walls, *Int. J. Numer. Methods Heat Fluid Flow*, vol. 22, no. 5, pp. 677–698, 2012.
- [20] D. Halliday, R. Resnick, and J. Walker, *Fundamentals of Physics Extended*, John Wiley & Sons, New York, NY, 2010.
- [21] B. Sreenivasan, P. A. Davidson, J. Etay, On the Control of Surface Waves by a Vertical Magnetic Field, *Phys. Fluids (1994-present)*, vol. 17, no. 11, pp. 117101, 2005.
- [22] J. N. Reddy, *An Introduction to the Finite Element Method*, McGraw-Hill, New York, 1993.
- [23] T. Basak, S. Roy, and A. Balakrishnan, Effects of Thermal Boundary Conditions on Natural Convection Flows Within a Square Cavity, *Int. J. Heat Mass Transfer*, vol. 49, no. 23, pp. 4525–4535, 2006.
- [24] T. Basak, S. Roy, T. Paul, and I. Pop, Natural Convection in a Square Cavity Filled with a Porous Medium: Effects of Various Thermal Boundary Conditions, *Int. J. Heat Mass Transfer*, vol. 49, no. 7, pp. 1430–1441, 2006.
- [25] C. Gau and R. Viskanta, Melting and Solidification of a Pure Metal on a Vertical Wall, *J. Heat Transfer*, vol. 108, no. 1, pp. 174–181, 1986.
- [26] R. Viswanath and Y. Jaluria, A Comparison of Different Solution Methodologies for Melting and Solidification Problems in Enclosures, *Numer. Heat Transfer Part B*, vol. 24, no. 1, pp. 77–105, 1993.
- [27] C. Desai and K. Vafai, A Unified Examination of the Melting Process within a Two-Dimensional Rectangular Cavity, *J. Heat Transfer*, vol. 115, no. 4, pp. 1072–1075, 1993.
- [28] A. Al-Mudhaf, and A. J. Chamkha, Natural Convection of Liquid Metals in an Inclined Enclosure in the Presence of a Magnetic Field, *Int. J. Fluid Mech. Res.*, vol. 31, no. 3, 2004.